Polarization-Modulated Infrared Spectroscopy and X-Ray Reflectivity of Photosystem II Core Complex at the Gas-Water Interface

Judith Gallant,* Bernard Desbat,# David Vaknin,§ and Christian Salesse*

*GREIB, Département de Chimie-Biologie, Université du Québec à Trois-Rivières, Trois-Rivières, Québec, Canada; #Laboratoire de Physicochimie Moléculaire, Université de Bordeaux I, 33405 Talence, France; and §Ames Laboratory, Physics Department, Iowa State University, Ames, Iowa 50011 USA

ABSTRACT The state of photosystem II core complex (PS II CC) in monolayer at the gas-water interface was investigated using in situ polarization-modulated infrared reflection absorption spectroscopy and x-ray reflectivity techniques. Two approaches for preparing and manipulating the monolayers were examined and compared. In the first, PS II CC was compressed immediately after spreading at an initial surface pressure of 5.7 mN/m, whereas in the second, the monolayer was incubated for 30 min at an initial surface pressure of 0.6 mN/m before compression. In the first approach, the protein complex maintained its native α-helical conformation upon compression, and the secondary structure of PS II CC was found to be stable for 2 h. The second approach resulted in films showing stable surface pressure below 30 mN/m and the presence of large amounts of β-sheets, which indicated denaturation of PS II CC. Above 30 mN/m, those films suffered surface pressure instability, which had to be compensated by continuous compression. This instability was correlated with the formation of new α-helices in the film. Measurements at 4°C strongly reduced denaturation of PS II CC. The x-ray reflectivity studies indicated that the spread film consists of a single protein layer at the gas-water interface. Altogether, this study provides direct structural and molecular information on membrane proteins when spread in monolayers at the gas-water interface.

INTRODUCTION

Photosystem II core complex (PS II CC) is a pigment-protein complex located in higher plant thylakoid membranes and is involved in the electron transport of the photosynthetic process (for reviews see Hanson and Wydrzynski, 1990; Nugent, 1996; Hankamer et al., 1997). PS II CC is the protein complex responsible for the photoinduced water oxidation that produces molecular oxygen as a by-product and is therefore essential to all animal life on earth. PS II CC consists of several hydrophobic and integral membrane polypeptides whose transmembrane spanning domains are believed to be mainly composed of α-helices (Vermaas et al., 1993). Integral polypeptides of PS II CC, shown in Fig. 1, include the 32- and 34-kDa reaction center (RC) proteins known as D1 and D2, the RC cytochrome b_{559}, containing two subunits of 9 and 4 kDa (Shuvalov, 1994), the chlorophyll (Chl)-binding internal antenna proteins CP47 and CP43 (approximately 47 and 43 kDa, respectively), and a number of smaller proteins whose sequence is known but whose function is still obscure. PS II CC also contains a 33-kDa extrinsic polypeptide that protects the binding site of water molecules involved in the oxidation process (Seidler, 1996). This water-binding site is a tetranuclear manganese cluster. The 33-kDa extrinsic polypeptide is necessary for stable oxygen evolution rates and is located exclusively on the luminal side of the thylakoid membrane. PS II CC also binds different cofactors and pigments, among which are Chls, pheophytins, and carotenoids. These pigments are involved in the collection and funneling of the light energy that ultimately reaches the RC where the initial charge separation occurs. This charge separation among pigments in the RC induces the photosynthetic water oxidation activity of PS II as well as the reduction of plastoquinones (Q_B) to plastoquinols. In thylakoid membranes, PS II CC is also associated with the light-harvesting complex (LHC). This complex is a mobile antenna that controls the light energy distribution between PS II and the following electron pump of the photosynthetic process, namely, photosystem I.

Membrane proteins, such as the proteins of the photosynthetic apparatus, are known to crystallize preferentially in two-dimensional (2D) arrays (Kühlbrandt et al., 1994). One possible means to attain this critical organization is through the use of Langmuir films (Uzgiris and Kornberg, 1983). Indeed, 2D monomolecular films provide an organization that facilitates contacts between oriented molecules, which are necessary to induce crystallization by reducing the degrees of freedom of molecules to two dimensions. Furthermore, the 2D protein concentration can be modified using lateral compression, and subphase components can be easily adjusted to optimize the film quality. Even though numerous studies were devoted to the 2D crystallization of PS II in the last decade (Seibert et al., 1987; Bassi et al., 1989; Fotinou et al., 1993; Holzenburg et al., 1996; Marr et al., 1996; Nakazato et al., 1996; Tsiotis et al. 1996; Morris et al., 1997; and references therein), the 3D structure of PS II CC is still unknown. Also, the resolution reached until now

Received for publication 20 November 1997 and in final form 28 August 1998.

Address reprint requests to Dr. Christian Salesse, Département de Chimie-Biologie, Université du Québec à Trois-Rivières, 3351 Boulevard des Forges, C.P. 500, Trois-Rivières, Québec, Canada G9A 5H7. Tel.: 819-376-5077; Fax: 819-376-5057; E-mail: christian_salesse@uqtr.uquebec.ca.

0006-3495/98/12/2888/12 $2.00

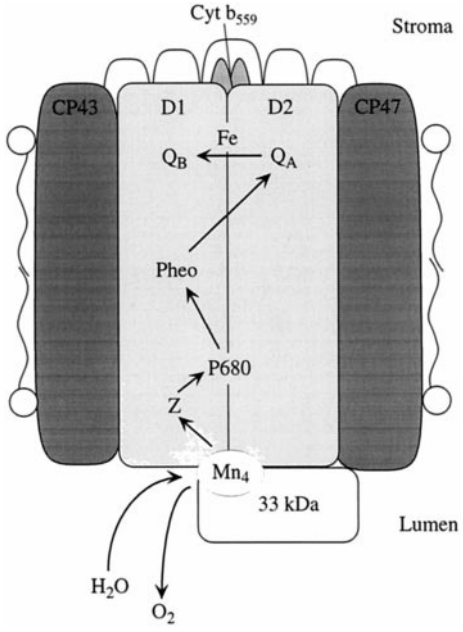

FIGURE 1 Schematic representation of PS II CC. The reaction center (RC) contains the polypeptides D1 and D2 and the two subunits of cytochrome b_{559}. Those polypeptides bind the following co-factors: the redox-active tyrosine Z, the RC primary electron donor P680 (chlorophyll), pheophytin (Pheo), plastoquinones (Q_A and Q_B), and a nonheme iron. CP47 and CP43 are chlorophyll *a* binding proteins that act as intrinsic antenna. The extrinsic 33-kDa polypeptide, essential for high oxygen evolution rates, protects the tetramanganese cluster, which is the water binding site. The hydrophobic part of PS II CC is approximately located at the same position as the detergent alkyl chains.

with these 2D crystals was limited to 20 Å. Our monolayer crystallization approach could improve this resolution. With the recent development of in situ x-ray grazing incidence diffraction using 2D protein crystals formed at the gas-water interface (Haas et al., 1995), it is now possible to investigate 2D protein crystals in situ and without the use of heavy atom staining. However, before reaching the ultimate phase of 2D crystal formation, one must carefully characterize and especially control protein structural organization and find the proper conditions to prepare monolayers where proteins remain native.

In the present work, we demonstrate with the help of polarization-modulated infrared reflection absorption spectroscopy (PM-IRRAS) the effect of different experimental conditions on PS II CC secondary structure in situ at the gas-water interface. PM-IRRAS is known to improve the infrared signal sensitivity of spread molecules at the interface, using a polarization modulation that reduces the strong anisotropic water interference in the amide I and II region of the infrared spectra (Blaudez et al., 1996). This technique provides information regarding the conformation and orientation of proteins at the interface. The intensity and position of PS II CC amide I and II bands were used to get insight into the α-helix and β-sheet content of this protein at the gas-water interface. We have also investigated the state of PS II CC monolayers using x-ray reflectivity measurements directly at the gas-water interface. This technique gives the electron density across the interface from which average thickness and molecular densities can be obtained. Comparing the thickness parameter with published dimensions of PS II CC obtained by electron microscopy enabled us to discriminate between mono-, bi-, or multilayer organization in these films.

MATERIALS AND METHODS

Purification and characterization of photosystem II core complex

PS II CC was extracted and purified from fresh spinach leaves using the method of van Leeuwen et al. (1991) with slight modifications. Isolation of PS II CC from LHC was performed at 4°C by fast protein liquid chromatography (FPLC) using a HiLoad 16/10 Q Sepharose high-performance column (Pharmacia Biotech, Uppsala, Sweden). Approximately 20 ml of the extract containing both PS II CC and LHC corresponding to a total of 35 mg of Chls was loaded onto the ion exchange column. LHC was eluted from the column until the eluate became nearly colorless, which took 30 min at a flow rate of 3 ml/min. After complete elution of LHC, PS II CC was eluted by increasing the concentration of $MgSO_4$ as described by van Leeuwen et al. (1991). The sample buffer used to prepare PS II CC contained 20 mM bis(2-hydroxyethyl)imino-tris(hydroxymethyl)methane (Bis-Tris, Sigma Chemical Co., St. Louis, MO) at pH 6.5, 20 mM $MgCl_2$ (Fisher Scientific Co., Fair Lawn, NJ), 5 mM $CaCl_2$ (Omega Chemical Co., Quebec, Canada), 75 mM $MgSO_4$ (Sigma), 400 mM sucrose (ACP Chemicals, Montreal, Canada), and 0.03% (w/v) *n*-dodecyl-β-D-maltoside (Calbiochem, San Diego, CA). The total procedure, from leaves to pure PS II CC fractions, took approximately 6 h. Samples were aliquoted, frozen in liquid nitrogen, and stored at -80°C until use.

Several methods were used to characterize PS II CC to evaluate its integrity. Chl concentration was measured by absorption spectroscopy as described by Porra et al. (1989). The chl *a*/chl *b* ratio of PS II CC samples was 11. Samples showing a lower chl *a*/chl *b* ratio were discarded as the presence of higher amounts of chl *b* indicate that CP29, a PS-II-associated intermediate antenna, was contaminating the samples. Functional intactness was verified by measuring light-saturated rates of oxygen evolution with a Clark-type electrode at 20°C (Hansatech, Norfolk, UK). During measurements, total Chl concentration was 5 μM, and 1 mM 2,5-dichloro-*p*-benzoquinone was used as electron acceptor (Pfaltz and Bauer, Waterbury, CT). The oxygen evolution rate of PS II CC was 1030 $\pm$ 90 μmol of O_2/mg of Chl per hour. Samples showing oxygen evolution rates lower than 1000 μmol of O_2/mg of Chl per hour were discarded. Assuming that there is one cyt b_{559} per PS II CC (MacDonald et al., 1994; Rögner et al., 1996), the concentration of PS II CC samples was determined by measuring its cyt b_{559} content, as described by De Las Rivas et al. (1995). This method consists in measuring the difference spectrum between the reduced (dithionite) and oxidized (ferricyanide) form of cyt b_{559} using an extinction coefficient of 17.5 mM^{-1} cm^{-1} at a Chl concentration of 0.1 mM. The determination of polypeptide composition of PS II CC was carried out by electrophoresis using published experimental conditions (Haag et al., 1990). PS II CC was diluted five times into the sodium dodecyl sulfate polyacrylamide gel electrophoresis (SDS-PAGE) sample buffer, and a volume of 10 μl was deposited on top of the stacking gel. Gels were run at 200 V for 50 min and were Coomassie stained. Polypeptides were identified using SDS-PAGE low-range molecular weight standards (Bio-Rad Laboratories, Mississauga, Canada). SDS-PAGE of our PS II CC preparations indicated the presence of CP47, CP43, D1, D2, cyt b_{559}, and the extrinsic 33-kDa polypeptide.

Film formation

The specific resistivity of ultrapure water was 18×10^6 Ω cm (Milli-Q, Millipore, Bedford, MA). In all reported experiments, the subphase used

contained 10 mM tris(hydroxymethyl)aminomethane buffer (Tris, Boehringer Mannheim, Laval, Canada) at pH 8, 500 mM NaCl (Ultrapure, J. T. Baker, Toronto, Canada), and 2 mM ascorbic acid (Fisher Scientific Co., Fair Lawn, NJ). Tris and NaCl were purified by chloroform extraction (Megasolv-HPLC 99.98%, Omega Chemical Co.) (Lamarche, 1988). This purification procedure consisted of a chloroform extraction of concentrated Tris (1 M) or NaCl (5.3 M) solutions. Surface active contaminants formed a gray film at the $CHCl_3$/water interface, which was eluted out with the organic phase. Additional extractions were performed until no more film was observed, and purification was completed by two final washes. The method of Trurnit (1960) was used to spread drops of PS II CC at the gas-water interface. All experiments were performed under dim green light. In all calculations, we used a PS II CC molecular mass of 240 kDa (Boekema et al., 1995).

Attenuated total internal reflectance (ATR) infrared spectroscopy

Fourier transform infrared (FTIR) spectra of PS II CC and its buffer were measured from 4000 to 650 cm^{-1} with a Nicolet Magna-IR 850 spectrometer (Madison, WI) equipped with a liquid-nitrogen-cooled HgCdTe detector and a Ge-coated KBr beam splitter. PS II CC was deposited on a Ge 45° parallelogram ATR crystal (50 mm × 20 mm × 2 mm). Excess water was evaporated under a gentle nitrogen stream before the crystal was placed in the analysis compartment. For each spectrum, 200 scans were collected with a 2-cm^{-1} resolution.

PM-IRRAS measurements

The home-made Langmuir trough used in the PM-IRRAS set up was made of aluminum and covered with a sheet of adhesive-precoated Teflon (Johnston Industrial Plastics, Lachine, Canada). Its width and length were 121 and 767 mm, respectively. The use of such a large trough was necessary to get a compression factor of 38.5, which allowed us to measure the entire isotherm of PS II CC. The trough's depth was 6 mm. Surface pressure (π) was detected with a Nima Wilhelmy plate system (Coventry, UK) using a Whatman chromatographic filter paper (Maidstone, UK) (Albrecht, 1983). The PS II CC sample concentration used in PM-IRRAS measurements was 12.7 ± 0.3 μM. Two initial surface pressures of 0.6 ± 0.1 and 5.7 ± 0.2 mN/m were obtained by spreading 20 or 40 μl, respectively, and three compression rates of 10, 40, and 80 nm^2/molecule min were investigated. When PS II CC was spread at 0.6 mN/m, the monolayer was incubated for 30 min before compression. Monolayers were always kept under nitrogen to prevent hazardous contact of molecular oxygen with our sample, and temperature was maintained at 24 ± 1°C, unless otherwise stated.

The complete optical setup and equations for PM-IRRAS measurements were described previously (Blaudez et al., 1996). Briefly, FTIR spectra were measured using a Nicolet 740 spectrometer. A polarizer was used to polarize the incident infrared beam, and the polarization was alternatively modulated between p- and s-linear states (parallel and perpendicular to the interface normal) with a ZnSe photoelastic modulator (Hinds type III, Portand, OR). The polarization modulation frequency was set at 2500 cm^{-1} to adequately investigate the infrared domain from 2000 to 1000 cm^{-1}. The reflected beam was finally focused on a liquid-nitrogen-cooled HgCdTe dectector (SAT, Poitier, France). Unless otherwise stated, 300 scans were collected for each spectrum at 4-cm^{-1} resolution. To quantify amide I and amide II as well as CH_2 and CH_3 band intensity variations, all spectra were decomposed between 1800 and 1350 cm^{-1}. Decompositions were performed using PeakSolve 1.01 (Galactic Industry Corp., Salem, NH). We optimized parameters so that all possible secondary structures would have an associated band in the amide I region and so that each visible band would have a component. In the case of intense spectra, calculations converged after less than 20 iterations. Correlation factors between decompositions and experimental data varied from 0.97 to 0.99.

X-ray reflectivity measurements

X-ray reflectivity measurements of the spread films were carried out in situ, on a liquid-surface x-ray reflectometer at Ames Laboratory. The apparatus is similar to the one developed by Als-Nielsen and Pershan (1983) with the additional capability to apply second-order corrections to the θ and the 2θ angles of the monochromator to ensure operation with a constant wavelength at all scattering angles. An x-ray beam of wavelength $\lambda = 1.5404$ Å was selected by Bragg reflection from the (111) planes of a single crystal Ge monochromator. The incident beam divergence was regulated by two adjustable slits in front of the sample, and the intensity of the incident beam was continuously monitored to account for possible fluctuations of the x-ray generator. To reduce surface waves during measurements, a glass plate was positioned in the trough under the x-ray beam footprint. The subphase depth above the glass plate was kept at approximately 300 μm. A dynamic vibration isolation system (JRS MOD-2, Affoltern, Switzerland) was used to remove mechanical vibrations. The Langmuir trough was contained in an airtight aluminum receptacle with Kapton windows, and its temperature was constantly maintained at 18°C. The sealed container was flushed with helium for 1 h before the beginning of the x-ray measurements, to reduce background due to air scattering and to protect the spread proteins from oxidation. Gas flow was allowed during compression of the monolayer to the required surface pressure, and it was stopped during x-ray data collection. To evaluate the film characteristics, 10 μl of an 8.7 ± 0.5 μM PS II CC solution was spread onto the subphase. To reduce the risks of protein unfolding, the compression was started immediately after spreading.

RESULTS AND DISCUSSION

Infrared spectroscopy

As spreading of PS II CC in monolayers at the gas-water interface could lead to protein denaturation, ATR-FTIR spectra of PS II CC were measured to get spectra of the native complex. Fig. 2 shows the ATR-FTIR spectrum of PS II CC. The water bands were subtracted using the buffer spectra with the algorithm published by Dousseau et al. (1989). ATR spectra below 1500 cm^{-1} are not shown because of intense bands appearing in that spectral domain that were attributed to the detergent. We observed the typ-

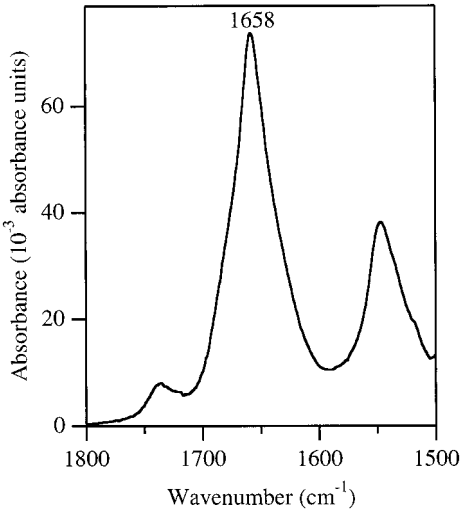

FIGURE 2 FTIR-ATR spectra of PS II CC spread as a hydrated amorphous thin film on a Ge crystal.

ical C═O ester carbonyl band at 1737 cm^{-1}, which is due to the presence of Chls and lipids in the sample (Katz et al., 1966; Chapados et al., 1990, 1991). The amide I band is centered at 1658 cm^{-1}. Correlations have been made in the literature between the position of the amide I band and the protein secondary structure (Jackson and Mantsch, 1995). It has been shown that α-helices are commonly observed between 1648 and 1660 cm^{-1}. The position of our amide I band at 1658 cm^{-1} thus confirmed the expected α-helical structure of PS II CC. To our knowledge, no other infrared spectrum of PS II CC can be found in the literature to compare with these data. The width and shape of this band indicate the presence of β-sheets. However, as PS II CC should be at least partially oriented with respect to the Ge ATR crystal, no attempt was made to deconvolute this amide I band to estimate the accurate secondary structure of the complex. Indeed, an optically anisotropic sample modifies the observed infrared intensities as the transition moments of the structural elements oriented parallel to the crystal surface have different intensities than those oriented perpendicular to the crystal. Shape and intensity of the band also depend on the angle of incident beam with respect to the crystal. Therefore, our result does not allow us to further discuss the relative content in α-helices and β-sheets of PS II CC. However, it clearly appears that the major vibrational contribution to the amide I band are α-helices.

PM-IRRAS

Compression speed has no effect on the structure of intact PS II CC

We investigated possible effects of different compression speeds on the structure of intact PS II CC. To maintain the integrity of PS II CC in monolayer, we spread the protein complex at an initial surface pressure of 5.7 mN/m and compressed the film immediately. Fig. 3 *A–C* shows PM-IRRAS spectra of PS II CC obtained at three different compression speeds and results of spectral decompositions are summarized in Table 1. These PM-IRRAS spectra are similar to published FTIR spectra of PS II RC, which contain 67% α-helices (He et al., 1991) as well as to infrared spectra of native PS II membrane particles (Chapados et al., 1990, 1991). From Fig. 3, it can be seen that the compression speed has very little influence on the overall shape of the spectra. At all compression speeds, PM-IRRAS signal increased with surface pressure, suggesting an increase in PS II CC surface concentration. All spectra show the C═O ester carbonyl band at 1737 cm^{-1}, due to Chls and lipids, as seen in the ATR spectrum (Fig. 2). Also, all spectra show an amide I band centered at approximately 1655 cm^{-1} (major component at 1657 cm^{-1}), indicating that the structure of PS II CC mainly contains α-helices (see Table 1). In addition, a small shoulder appearing at approximately 1630 cm^{-1} (component at 1627 cm^{-1}) can be observed in all spectra, indicating the presence of β-sheets. We believe that this shoulder may be due, at least partly, to the presence of the extrinsic 33-kDa polypeptide, thus suggesting that this extrinsic protein is still anchored to the complex after spreading at the gas-water interface. Indeed, the extrinsic 33-kDa polypeptide is known to contain between 36 and 50% β-sheets (Xu et al., 1994; Ahmed et al., 1995; Zhang et al., 1996). The fact that it is better observed by PM-IRRAS compared with ATR spectra may be due to a difference in orientation of PS II CC with respect to the measuring beam that slightly favors its observation in the PM-IRRAS spectra.

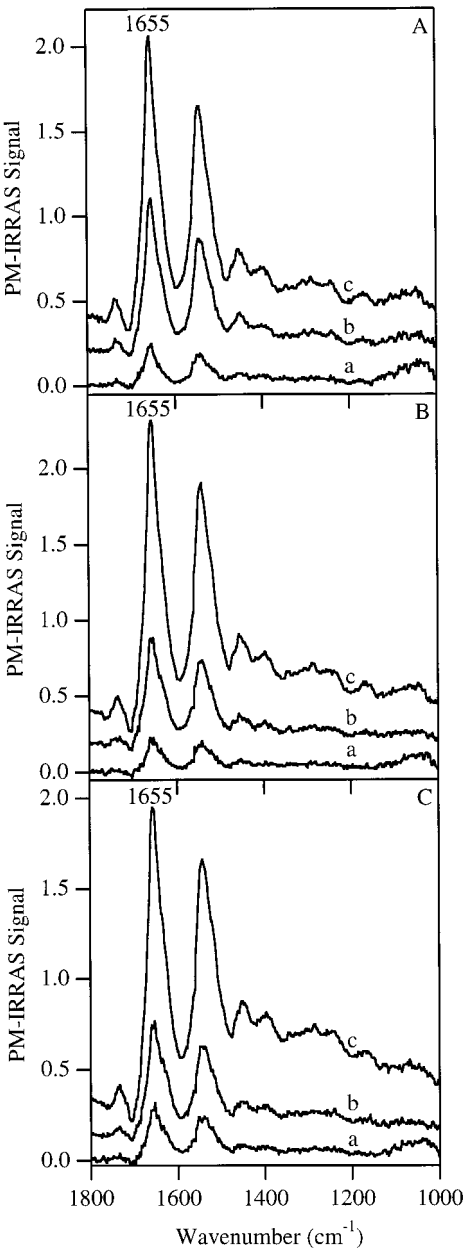

FIGURE 3 PM-IRRAS spectra of PS II CC monolayers at the nitrogen-water interface. Initial surface pressure was set at 5.7 ± 0.2 mN/m. Compression at 80 nm^2/molecule min (*A*), 40 nm^2/molecule min (*B*), and 10 nm^2/molecule min (*C*) was started immediately after spreading of 40 μl of PS II CC. Spectra were measured at surface pressures of 10 mN/m (*a*), 20 mN/m (*b*), and 30 mN/m (*c*).

TABLE 1 Effect of initial surface pressure, compression speed, and surface pressure on PS II CC secondary structure and orientation at the gas-water interface

π_i (mN/m)	Compression speed (nm^2/molecule min)	π (mN/m)	% α-helices	% β-sheets	AI/AII ratio
5.7	80	10	68	11	1.4
		20	69	15	1.1
		30	71	12	1.2
5.7	40	10	61	29	1.6
		20	64	20	1.4
		30	70	15	1.3
5.7	10	10	62	22	1.3
		20	66	22	1.4
		30	63	19	1.4
0.6	80	0.6	29	71	1.1
		10	33	67	0.9
		20	36	64	1.1
		30	35	60	1.1
		40	49	29	1.2
0.6	40	0.6	28	53	1.3
		10	28	59	1.3
		20	28	66	1.2
		30	29	64	1.4
		40	38	42	1.1
0.6	40 (4°C)	0.6	60	6	4.4
		10	55	15	3.4
		20	54	24	2.4
		30	48	27	2.2
		40	48	22	1.6
0.6	10	0.6	18	82	0.9
		10	25	75	1.0
		20	19	79	0.9
		30	23	75	1.0
		40	26	60	1.0

π_i, initial surface pressure; π, surface pressure; % α-helices, percentage of α-helices in the amide I band; % β-sheets, percentage of β-sheets in the amide I band; AI/AII ratio, ratio of amide I to amide II bands.

Table 1 shows a summary of the relative content in α-helices and β-sheets obtained from spectral decomposition of PM-IRRAS spectra. As PM-IRRAS is sensitive to the orientation of secondary structures, these data are only indications of relative proportions and changes occurring in the films and should not be interpreted as exact values. It can be seen in Table 1 that the native α-helical secondary structure of PS II CC was maintained when the initial surface pressure was 5.7 mN/m, with an average of 66% α-helices and 18% β-sheets. The amide I/amide II ratio (AI/AII) was used to estimate the relative orientational changes of PS II CC taking place as a function of surface pressure. Indeed, it was previously reported (Cornut et al., 1996) that AI/AII ratio varies from 6.5 to -1 when α-helices are oriented parallel and perpendicular to the gas-water interface, respectively. Similar changes are also observed in the case of β-sheet reorientation (to be reported elsewhere). Therefore, the combination of AI/AII ratio and the relative content in α-helices and β-sheets allowed us to discriminate between either conformational changes taking place during compression (small changes in AI/AII ratio and large changes in relative secondary structure content) or reorientation of PS II CC (changes in both AI/AII ratio and relative secondary structure content). Although the AI/AII ratio does not change linearly with α-helix angle, on average, a variation of 1 in AI/AII corresponds to a 12° change in orientation. Table 1 shows that when PS II CC was spread at an initial surface pressure of 5.7 mN/m, compression speed did not affect the structure of the complex as both relative secondary structures and values of AI/AII ratio remained almost unchanged.

Intensity of the amide I band

At 30 mN/m, PM-IRRAS spectra of PS II CC showed maximal amide I intensities ranging from 1.60 to 1.91 (Fig. 3). These intensities were compared with those of rhodopsin (Rho) and bacteriorhodopsin (bR) under similar protein surface density. In the case of Rho, maximal amide I intensity was 0.66, whereas bR showed a maximum of 0.40 (to be published elsewhere). The amide I bands of PS II CC monolayers were thus 2.4–4.8 times more intense than those of Rho or bR, respectively. It was previously shown that the intensity of the amide I band in PM-IRRAS spectra is sensitive to the orientation of α-helices (Cornut et al., 1996), where the surface-lying α-helices produce the strongest amide I bands. Models of Rho and bR each show three α-helices oriented nearly perpendicular to the membrane plane and four slightly tilted helices (Schertler and Hargrave, 1995). In contrast, models of PS II CC show that several polypeptides, among which D1 and D2 (Svensson et al., 1990, 1996; Xiong et al., 1996) contain some α-helices that are oriented approximately parallel to the membrane surface (perpendicular to the interface normal). Therefore, the presence of those surface-lying helices may explain the high amide I signal observed for PS II CC monolayers, compared with those of Rho and bR.

Evidence for the elimination of the excess detergent into the subphase

In all spectra of intact PS II CC taken at 10 mN/m (spectra *a* in Fig. 3 *A–C*), we noticed the presence of numerous bands in the 1150–1000 cm^{-1} region, which had a relative intensity of approximately one-half that of the amide I band. The relative intensity of these bands compared with the amide I band decreased with surface pressure as can be seen in Fig. 4 which shows normalized PM-IRRAS spectra at 10 and 30 mN/m (spectra *a* and *b*, respectively). The most intense C—O stretching bands of the detergent, *n*-dodecyl-β-D-maltoside, are located in that frequency domain (not shown). We thus believe that the decreased intensity of these bands with surface pressure is due to the detergent solubilization into the subphase. The removal of this excess detergent is a great advantage for further crystallization studies. Indeed, 2D crystals of membrane proteins are usually formed by preparing lipid vesicles containing high concentrations of these proteins in which excess detergent is removed by dialysis.

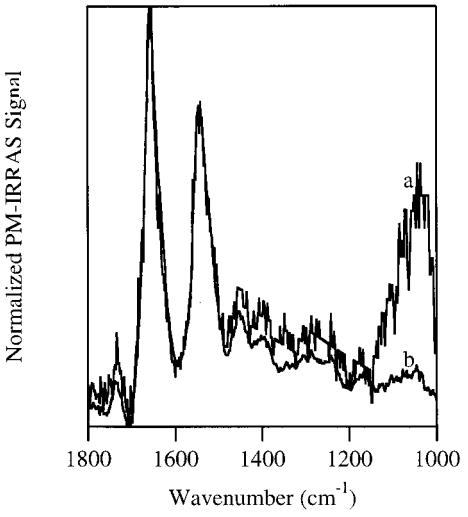

FIGURE 4 Comparison of normalized PM-IRRAS spectra of PS II CC monolayers at the nitrogen-water interface spread at an initial surface pressure of 5.7 ± 0.2 mN/m. Compression at 80 nm^2/molecule min was started immediately after spreading of 40 μl of PS II CC. Spectra were measured at 10 mN/m (*a*) and 30 mN/m (*b*).

Surface pressure has no effect on the structure of intact PS II CC

We examined the possibility that the structure and orientation of PS II CC change upon compression to higher surface pressures. To visualize those changes, if any, we compared normalized spectra of PS II CC monolayers, at 10 and 30 mN/m, when spread under similar conditions. One example of this comparison is shown in Fig. 4. The higher noise level in the 10 mN/m spectrum (spectrum *a*) is due to the reduced protein interfacial concentration at this surface pressure. It can be seen that the shape of the amide I and II bands are very similar. Moreover, the corresponding data in Table 1 suggest that the secondary structure of PS II CC remains almost unchanged with compression. In addition, the AI/AII ratio is very similar at these two surface pressures (see Fig. 4 and Table 1). It is thus clear from these spectra that compression to higher surface pressures affected neither the α-helix content nor the orientation of PS II CC with respect to the interface normal.

Stability of the α-helix secondary structure

With the aim of preparing PS II CC 2D crystals, we investigated the stability of PS II CC monolayers at room temperature as a function of time. Therefore, we measured PM-IRRAS spectra of PS II CC at a surface pressure of 20 mN/m every 15 min for a period of 2 h (Fig. 5). During the first 30 min (spectra *a* and *b*), it was necessary to compress the film to compensate for the reduction in surface pressure. After 30 min, the surface pressure of the film was stabilized. This decrease in surface pressure was interpreted in terms of solubilization of some material into the subphase, presumably the detergent, as shown in Fig. 4 (see above). Also, the

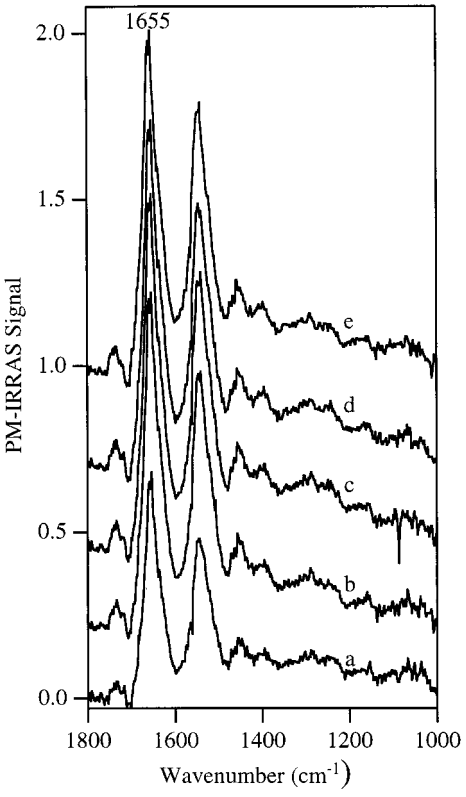

FIGURE 5 PM-IRRAS spectra of PS II CC monolayers at the nitrogen-water interface. Initial surface pressure was set at 5.7 ± 0.2 mN/m. Compression at 80 nm^2/molecule min was started immediately after spreading of 40 μl of PS II CC. Surface pressure was maintained at 20 mN/m. Spectra were measured at 15 min (*a*), 30 min (*b*), 45 min (*c*), 75 min (*d*), and 120 min (*e*) after reaching 20 mN/m.

first spectrum, taken in the first 15 min after spreading (spectrum *a*, Fig. 5), has an amide I intensity 38% lower than the ones taken at times ranging from 30 to 120 min after spreading. This observation also supports our detergent solubilization hypothesis. In fact, when the detergent is leaving the interface, the PS II CC concentration in the film is rising, thus increasing the amide I intensity. When the surface pressure was stabilized, there was no more increase in the amide I intensity. The most important observation from Fig. 5 was that all amide I bands remained centered at 1655 cm^{-1} (major component at 1657 cm^{-1}). In fact, the secondary structure content of PS II CC remained almost unchanged with an average of 70 ± 2% α-helices (data not shown). We therefore concluded that PS II CC maintained its α-helical structure during the 2-h incubation time at the gas-water interface at 20 mN/m and that no time-dependent denaturation was observed.

Effect of low-surface-pressure incubation on PS II CC structure

Many publications discussed the probable effect of incubation at low surface pressure on either bacterial RC or PS II RC (Tiede, 1985; Alegria and Dutton, 1991; Yasuda et al.,

1992; Uphaus et al., 1997). However, none of those studies provide molecular information on protein unfolding at the gas-water interface. Therefore, we further investigated the effect of incubation at low surface pressure and of different compression speeds on PM-IRRAS spectra of PS II CC as shown in Fig. 6.

Formation of β-sheets

We observed that PS II CC secondary structure was altered by the low-surface-pressure treatment (see spectra *a–d*, Fig. 6 *A–C*). Indeed, unfolding of PS II CC at the gas-water interface modified the native α-helical structure of the protein and produced β-sheets. This interpretation is confirmed by the amide I band position, located at 1629 cm^{-1}, which was due to an underlying component located at 1627 cm^{-1}, characteristic of β-sheets (Jackson and Mantsch, 1995). Indeed, the data reported in Table 1 show an average of 28 ± 6% α-helices and 68 ± 9% β-sheets, at surface pressures equal or lower than 30 mN/m. It is noteworthy that these values are inverted compared with those measured at 5.7 mN/m (see Table 1).

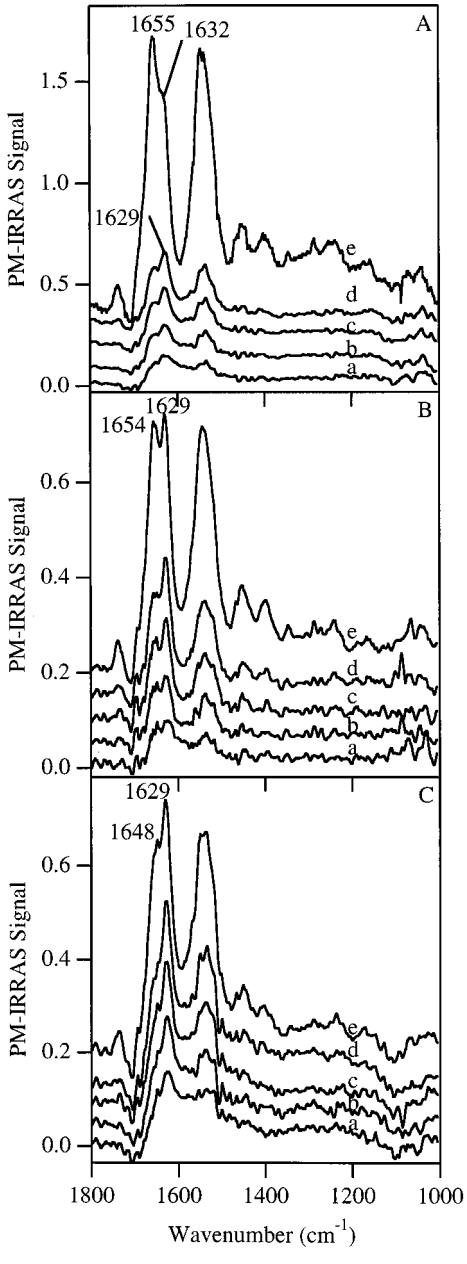

FIGURE 6 PM-IRRAS spectra of PS II CC monolayers at the nitrogen-water interface. Initial surface pressure was set at 0.6 ± 0.1 mN/m. Compression at 80 nm^2/molecule min (*A*), 40 nm^2/molecule min (*B*), and 10 nm^2/molecule min (*C*) was started 30 min after spreading of 20 μl of PS II CC. Spectra were measured at 0.6 mN/m (*a*), 10 mN/m (*b*), 20 mN/m (*c*), 30 mN/m (*d*), and 40 mN/m (*e*).

We also observed that the intensity of the amide I band corresponding to β-sheets is much lower than what was previously observed for α-helices (compare Figs. 3 and 6). This reduction was attributed to the fact that unfolded β-sheets occupy a larger area at the interface than α-helices. Indeed, the measurement of surface pressure-area isotherms showed that incubation of PS II CC at 0.6 mN/m leads to an increase of 1.7–4.3 in molecular area compared with when it is spread at 5.7 mN/m (Gallant et al., 1998). The PM-IRRAS signal is thus lowered as the number of amino acid residues per surface area is reduced. Finally, we also noticed that the film was extremely stable at surface pressures lower than 30 mN/m. Indeed, no compression was needed to maintain the film at the desired surface pressure during PM-IRRAS measurements in contrast to what was observed in Fig. 5 (see above). This behavior is due to the fact that the excess detergent is lost during the 30-min incubation time rather than during compression (Gallant et al., 1998).

Effect of surface pressure and compression speed on β-sheets at surface pressures up to 30 mN/m

The general shape of PM-IRRAS spectra of denatured PS II CC did not change substantially upon compression as long as the film was maintained at pressures equal to or lower than 30 mN/m. This means that compression did not alter the β-sheet content of PS II CC in that range of surface pressures. As an example, it can be seen that spectra *a–d* in Fig. 6 A showed no major difference upon compression. The secondary structure content showed 33 ± 3% α-helices and 65 ± 5% β-sheets (Table 1). The same phenomenon was observed at other compression speeds (see spectra *a–d*, Fig. 6, *B* and *C*, as well as Table 1). At 40 and 10 nm^2/molecule min, the average content of α-helices and β-sheets were 28 ± 1 and 60 ± 6%, and 21 ± 3 and 78 ± 3%, respectively. As expected, the intensity of the amide I band increased with surface pressure. This is due to the increase in surface concentration of the unfolded polypeptides as molecular area is decreased.

We observed a slight effect of compression speed on the film structure. Indeed, the slower compression speed produced a higher content in β-sheets than the two other compression speeds (78 ± 3% at 10 nm^2/molecule min versus 60 ± 6% and 65 ± 5% at 40 and 80 nm^2/molecule min, respectively). The near-equilibrium state in the film during compression at this slowest speed could have al-

lowed maintenance of the interactions between amino acid residues that form the β-sheets.

Formation of new α-helices at surface pressures higher than 30 mN/m

Whenever denatured films of PS II CC were compressed at surface pressures higher than 30 mN/m, we observed a noticeable and reproducible phenomenon. Indeed, no matter what compression speed was investigated, the surface pressure of denatured films became unstable. It systematically needed to be compensated continuously by compression during measurements, indicating that some type of reorganization of the film was taking place at the interface. In fact, PM-IRRAS spectra indicated that the protein secondary structure was considerably altered when the pressure reached 40 mN/m compared with 30 mN/m (see Fig. 6 *A–C* and Table 1).

Compression to 40 mN/m resulted in different protein conformations, depending on the speed of compression (compare spectra *e*, Fig. 6 *A–C*). When PS II CC was compressed at a speed of 10 nm^2/molecule min (spectrum *e*, Fig. 6 *C*), the amide I maximum remained centered at 1629 cm^{-1} (major component at 1627 cm^{-1}). This indicated that the film maintained its β-sheet structure upon further compression. The data in Table 1 indicate that at 40 mN/m, the secondary structure still contained 60% β-sheets, although this value was reduced compared with lower surface pressures (averaging 78 $\pm$ 3%). Indeed, when spectrum *e* (Fig. 6 *C*) is compared with the one measured at 30 mN/m (spectrum *d*, Fig. 6 *C*), we noticed that a stronger band appeared at 1648 cm^{-1}, which indicated that the protein film underwent a minor secondary structure change, with a slight reduction of the β-sheet content allowing the probable formation of some random coils. Nevertheless, at this low speed of compression, the film maintained a large β-sheet content.

In contrast, when the film was compressed at high speed (80 nm^2/molecule min), as shown by spectrum *e* in Fig. 6 *A*, a clear and reproducible change in the secondary structure of denatured PS II CC occurred from 30 to 40 mN/m. The amide I maximum shifted from the original 1629 cm^{-1} (spectrum *d*) to 1655 cm^{-1} (spectrum *e*), which was interpreted as the formation of new α-helices, although the shoulder at 1632 cm^{-1} indicated that the film still contained an important portion of β-sheets. Indeed, the β-sheet content was reduced from 65 $\pm$ 5% to 29%, whereas the α-helix content rose from 33 $\pm$ 3% to 49% (see Table 1). Another feature was observed at 40 mN/m compared with 30 mN/m, where a very large increase in the amide I intensity is observed (compare spectra *d* and *e*, Fig. 6 *A*). Although it did not quite reach intensities found in intact films of PS II CC (see Fig. 3), this increase suggests that large amounts of new α-helices were formed. This is, to our knowledge, the first evidence of a surface-pressure-induced and compression-speed-controlled reversible secondary structure change of proteins at the interface.

The spectrum *e* of Fig. 6 *B* shows one of the spectra obtained when unfolded PS II CC films were compressed at 40 nm^2/molecule min. At that particular compression speed, various unreproducible spectra were obtained at a surface pressure of 40 mN/m. Indeed, under this experimental condition, we obtained spectra as those shown in Fig. 6, *A* or *C*. The one illustrated in Fig. 6 *B* was a frequently observed behavior. We found no explanation for why the content of α-helices and β-sheets varied from one experiment to another in this specific experimental condition.

The molecular processes affecting the structure of PS II CC films at low surface pressure may be compression speed dependent. In the case of the low compression speed (10 nm^2/molecule min, Fig. 6 *C*), the system was probably close to a near-equilibrium state. As the time needed to reach the surface pressure of 40 mN/m was four to eight times longer, the unfolded protein could behave differently compared with when it was rapidly compressed at 40 or 80 nm^2/molecule min (Fig. 6, *B* and *A*, respectively). When compressed at 10 nm^2/molecule min, the β-sheets could have adapted to the slowly rising pressure by changing their relative packing up to the point where the pressure finally reached 40 mN/m without any significant change in the secondary structure of the protein. However, when the film was compressed at 80 nm^2/molecule min, the fast compression could have triggered conformational changes of the unfolded protein, which responded to this abrupt pressure rise by an immediate formation α-helices, which corresponds to a more compact structure. It is interesting to mention the recent data of Dieudonné et al. (1998) on the secondary structure of synthetic peptides when spread in monolayers at the air-D_2O interface, which correlate well with our observations. They have indeed shown that the secondary structure adopted by their peptides depended remarkably on the initial surface pressure of spreading. They have also observed that their molecules were α-helical when spread at high surface pressures. Moreover, the relative intensity of bands initially observed after spreading one peptide was shown to vary considerably with increasing surface pressure similarly to our observation in Fig. 6 *A*.

State of PS II CC immediately after spreading

To probe the process of denaturation when PS II CC was spread at low surface pressure, PM-IRRAS spectra of PS II CC were measured immediately after spreading and compared with the one obtained after a 30-min incubation time at a surface pressure of 0.6 mN/m. These spectra are illustrated in Fig. 7. To obtain a band position that would represent the initial state of PS II CC right after spreading, the number of scans was reduced to 20, which corresponded to a measuring time of 1 min. The spectrum obtained (spectrum *a*, Fig. 7), although noisy, shows a distinct amide I band maximum at approximately 1654 cm^{-1}, indicating that 1 min after spreading, the protein complex still retained its α-helical structure. However, after 30 min of incubation at 0.6 mN/m (spectrum *b*, Fig. 7), the maximum was shifted

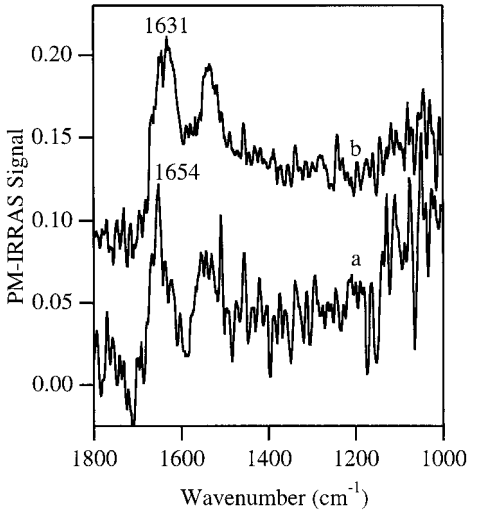

FIGURE 7 PM-IRRAS spectra of PS II CC monolayers at the nitrogen-water interface. Surface pressure was set at 0.6 ± 0.1 mN/m, and the film was not compressed. Spectra were recorded at 0 min (20 scans) (*a*) and 30 min (*b*) after spreading 20 μl of PS II CC.

to 1631 cm^{-1}, the characteristic band position of β-sheets. This indicates that the incubation time at low surface pressures is a critical factor in the denaturation of proteins at the interface as is the value of the initial spreading surface pressure.

Effect of low temperature on PS II CC

We also investigated the effect of low temperature on the denaturation process of PS II CC in monolayers at the gas-water interface. We therefore reduced the temperature of the subphase to 4°C. After 43 min of incubation of PS II CC at 0.6 mN/m, we measured a first spectrum and then started the compression at a speed of 40 nm^2/molecule min. Fig. 8 shows the results of those experiments, and the corresponding secondary structure content is listed in Table 1. It can be seen that the amide I band remained centered at 1655 cm^{-1}, with its major underlying α-helical component appearing at 1657 cm^{-1} and representing 60% of the secondary structure (at 0.6 mN/m). Therefore, these data suggested that under these conditions, which were previously shown to induce denaturation of PS II CC at room temperature (see Fig. 6 *B* and the corresponding data in Table 1), the protein complex preserved most of its α-helices, and thus, the extent of denaturation is largely reduced. However, it is also important to notice that the two shoulders located at 1632 and 1695 cm^{-1} indicate that there is a distinct fraction of PS II CC that exists in antiparallel β-sheet structure, which may be attributed, at least partly, to the extrinsic 33-kDa polypeptide (Ahmed et al., 1995).

Another important feature of these spectra is the observation of large changes in the AI/AII ratio at 4°C (Table 1). This is the only case where evidence is shown for the reorientation of PS II CC at the interface. Indeed, these variations of AI/AII ratio from 4.4 to 1.6 clearly indicate

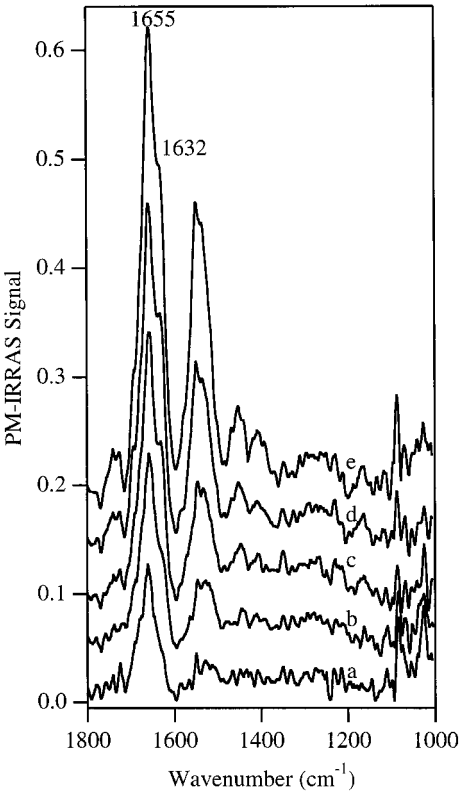

FIGURE 8 PM-IRRAS spectra of PS II CC monolayers at the nitrogen-water interface at 4°C. Initial surface pressure was set at 0.6 ± 0.1 mN/m. Compression at 40 nm^2/molecule min was started 43 min after spreading of 20 μl of PS II CC. Spectra were measured at 0.6 mN/m (*a*), 10 mN/m (*b*), 20 mN/m (*c*), 30 mN/m (*d*), and 40 mN/m (*e*).

that PS II CC is oriented differently at low compared with high surface pressures, with its α-helices lying more parallel to the monolayer plane (Table 1). These data suggest that with increasing surface pressure, α-helices are pushed upwards, thus reducing the AI/AII ratio. It is noteworthy that the AI/AII ratio of 1.6 at 40 mN/m is similar to other values reported in Table 1. Therefore, only the secondary structure content estimated at 40 mN/m can be compared with the other experimental conditions appearing in Table 1. The value of 48% α-helices obtained at 40 mN/m strongly suggests that lower temperature greatly reduced denaturation of PS II CC at the interface.

X-ray reflectivity

Fig. 9 shows an x-ray reflectivity curve normalized to the reflectivity of an ideally flat subphase (R/R_F) versus the momentum transfer (Q_Z) of a PS II CC monolayer maintained at 30 ± 1 mN/m. The solid line is the best-fit calculated reflectivity from the electron density model structure shown in the inset as a solid line. We started by modeling the reflectivity with a one-box model, which yielded unsatisfactory fit. Only by adding a second box was a better fit achieved. The reflectivity was thus calculated by assuming a two-box model (Als-Nielsen and Kjaer, 1989).

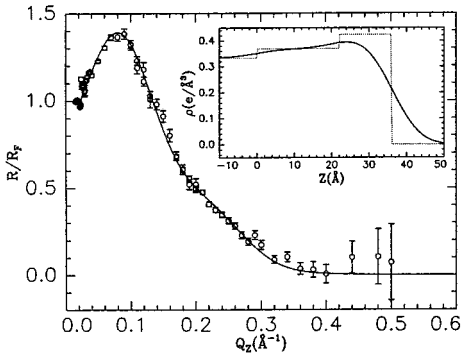

FIGURE 9 X-ray reflectivity (normalized to the Fresnel reflectivity R_F of ideally flat subphase) versus momentum transfer Q_z, of a PS II CC monolayer. The solid curve is the calculated reflectivity obtained from the scattering length density profile shown as a solid line in the inset. The dotted line in the inset corresponds to the box model that is smeared by a Gaussian to give the solid curve. Surface pressure was maintained at 30 mN/m during the measurement.

A recursive formalism (Parratt, 1954) was used to calculate the reflectivity from ideally flat interfaces, $R_0(Q_z)$. To account for surface roughness σ under the assumption of Gaussian smeared interfaces, a Debye-Waller factor was applied as follows:

$$R(Q_z) = R_0(Q_z)e^{-(Q_z\sigma)^2} \quad (1)$$

The dotted line in the inset corresponds to the box model in the absence of the effect of surface roughness. The thickness values of the two boxes extracted from the reflectivity are 22 ± 2 and 14 ± 2 Å with electron number densities of 0.37 ± 0.02 and 0.42 ± 0.02 e/Å^3, respectively, and a surface roughness σ = 5.9 ± 0.5 Å. The two-box model suggests that PS II CC may be composed of two distinct electron density zones. We hypothesize that the detergent trapped in the PS II CC monolayer, surrounding and stabilizing the complex, and/or any anisotropically distributed cofactors inside the complex may contribute to the apparent separate electron densities.

Surface roughness

The surface roughness of a pure liquid-vapor interface is dominated by thermally excited capillary waves, σ_{CW}, that depend on surface tension γ ($\sigma_{CW}^2 \propto k_BT/\gamma$). In addition, the effective surface roughness σ depends on the intrinsic roughness σ_I, due to the size, shape, and organization of the molecules at the interface. Therefore, the measured effective roughness from the reflectivity is given by (Ocko et al., 1994):

$$\sigma^2 = \sigma_{CW}^2 + \sigma_I^2 \quad (2)$$

For pure liquids, in particular for water, the intrinsic part is comparable or smaller than the capillary waves term. Under the vibration damping conditions described above (glass plate and dynamic anti-vibration system), the effective surface roughness from pure water (or subphase) is approximately 2.4–2.8 Å depending on the resolution of the spectrometer and the attenuation of waves at the interface. For typical Langmuir monolayers (i.e., fatty acids, lipids, etc.), there is a small increase in the surface roughness, which is usually associated with the increase of surface pressure (or equivalently the decrease in surface tension) as discussed above (Als-Nielsen and Kjaer, 1989). The effective surface roughness for these monolayers at moderate pressures (20–35 mN/m) is in the range 2.8–4 Å. In the present case, the roughness is too large to be accounted for by capillary waves only, and we argue that the roughness is dominated by the intrinsic part, which, using Eq. 2, is estimated at $\sigma_I \approx$ 4.5–5.5 Å. This larger intrinsic roughness can be associated with the irregularity inherent to the morphology of proteins. One reason for the increased surface roughness may be related to the presence of the hydrophilic loops that link together the transmembrane α-helices of PS II CC. These large luminal loops contain residues that play crucial roles in the interaction between transmembrane polypeptides and extrinsic oxygen evolving complex proteins and cofactors. On the other hand, the loops on the stromal side, which are shorter than those found on the luminal side, might interact with another PS II CC, producing either the aggregated structure observed in solution, which is similar to the stacking of PS II in thylakoid membranes in vivo. As these loops are not as well organized as α-helices and vary considerably in sizes, from 18 to 190 residues for CP47 alone, they probably are responsible for the external shape on the surface of the complex. Therefore, the surface roughness value is most probably affected by the presence of these loops.

Film thickness

The total homogeneous thickness of the film as extracted from the box model in the absence of surface roughness is 36 ± 4 Å, which is too small to account for the real size of PS II CC. This discrepancy is intimately related to the increase in surface roughness as discussed above. The larger roughness that we extracted for the film indicates that the protein protrudes into both the air-protein interface as well as the protein-water interface. Lateral heterogeneity on the molecular length scale could have been included partially in the model had the molecular form factor of the protein in the film been known. We argue that the thickness (d_{TOT}) of individual proteins in the film is better approximated as a sum of the homogeneous part (determined from the box model) and a cutoff length that depends on the intrinsic roughness σ_I. Assuming a cutoff that is twice the surface roughness at each interface (air-protein and protein-water interfaces) yields:

$$d_{TOT} \approx d_{box} + 4\sigma_I = 58 \pm 8 \text{ Å} \quad (3)$$

This result compares with previously published data for PS II CC obtained by electron microscopy (Boekema et al., 1995) of a 60-Å edge-to-edge thickness.

Monolayer versus bilayer

By examining the overall profile of the electron density (Fig. 9) and comparing it with known dimensions of PS II CC, we suggest that the film at the interface consists of a single protein layer. The stromal face-to-face aggregation, which is typically observed in solution as well as in thylakoid membranes, is most likely not occurring in monolayers at the gas-water interface. This aggregation would have given a film thickness of approximately 120 Å. The relatively high NaCl concentration of the subphase (500 mM) is probably responsible for the prevention of this type of aggregation of PS II CC. It is indeed known that the presence of large amounts of monovalent cations tends to induce the destacking of thylakoid membranes (Barber, 1980).

CONCLUSION

The investigation of PS II CC in monolayers has provided molecular information about the structure of this protein complex when spread at the gas-liquid interface. We have demonstrated that the spreading conditions are of particular importance to maintain the α-helical secondary structure of PS II CC. We also showed that conditions can be found to form stable monolayers, which could eventually allow 2D crystallization of PS II CC. When PS II CC is spread at an initial surface pressure of 5.7 mN/m and immediately compressed, the α-helical content of this complex is maintained. Although we also found experimental conditions, usually used to spread lipids, leading to the denaturation of PS II CC, the study of the molecular processes involved in protein denaturation is also of primary significance. Indeed, the fact that the protein conformation changed upon compression from 30 to 40 mN/m to form α-helices from β-sheets regardless of the compression rate is an interesting observation that implies some control on protein folding at the gas-water interface. Additional studies of this phenomenon could lead to a better understanding of protein folding in natural membranes.

The drastic decrease in protein denaturation upon reduction of temperature is definitely a promising new research avenue. As 2D crystallization may be favored by the reduction of temperature, owing to slower movements of spread molecules at the interface as well as water molecules, our results have shown that an additional advantage is the observation of lower rates of denaturation.

The thickness measured by x-ray reflectivity indicates that the film is composed of a single layer of protein homogeneously distributed at the interface. Additional studies at synchrotron radiation sources will enable a more detailed reflectivity study and, in addition, will provide information on the lateral organization of PS II CC and, in particular, of crystallized films.

Many investigators have previously raised hypotheses on the status of protein structure once spread in monolayers without any direct supporting evidence. This paper demonstrates the powerful capacity of infrared spectroscopy to provide direct stuctural information on membrane proteins when spread in monolayers at the air-water interface. Perhaps the most impressive result of this paper is the fact that it is possible to prepare monolayers of membrane proteins where its native secondary structure is maintained.

Special thanks are due to Sacha Bonenfant and Dr. Michel Pézolet at CERSIM for their help with the FTIR-ATR measurements.

We are indebted to the Natural Sciences and Engineering Research Council of Canada, the Fonds pour la Formation de Chercheurs et l'Aide à la Recherche, and FRSQ for financial support. J. G. was also supported by Le Syndicat des Chargé(e)s de Cours de l'Université du Québec à Trois-Rivières and the Fondation du CEU. Ames Laboratory is operated by Iowa State University for the Department of Energy under contract W-7405-Eng-82. The work at Ames was supported by the Director for Energy Research, Office of Basic Sciences. We are also indebted to NATO for a Collaborative Research grant.

REFERENCES

Ahmed, A., H.-A. Tajmir-Riahi, and R. Carpentier. 1995. A quantitative secondary structure analysis of the 33 kDa extrinsic polypeptide of photosystem II by FTIR spectroscopy. *FEBS Lett.* 363:65–68.

Albrecht, O. 1983. The construction of a microprocessor-controlled film balance for precision measurement of isotherms and isobars. *Thin Solid Films*. 99:227–234.

Alegria, G., and P. L. Dutton. 1991. Langmuir-Blodgett monolayer films of bacterial photosynthetic membranes and isolated reaction centers. I. Preparation, spectrophotometric and electrochemical characterization. *Biochim. Biophys. Acta.* 1057:239–257.

Als-Nielsen, J., and K. Kjaer. 1989. X-ray reflectivity and diffraction studies of liquid surfaces and surfactant monolayers. *In* Phase Transitions in Soft Condensed Matter. T. Riste and D. Sherrington, editors. Plenum Press, New York. 113–138.

Als-Nielsen, J., and P. S. Pershan. 1983. Synchrotron x-ray diffraction study of liquid surfaces. *Nucl. Instrum. Methods.* 208:545–548.

Barber, J. 1980. Membrane surface charges and potentials in relation to photosynthesis. *Biochim. Biophys. Acta.* 594:253–308.

Bassi, R., A. G. Magaldi, G. Tognon, G. M. Giacometti, and K. R. Miller. 1989. Two-dimensional crystal of the photosystem II reaction center complex from higher plants. *Eur. J. Cell Biol.* 50:84–93.

Blaudez, D., J.-M. Turlet, J. Dufourcq, D. Bard, T. Buffeteau, and B. Desbat. 1996. Investigations at the air/water interface using polarization modulation IR spectroscopy. *J. Chem. Soc. Faraday Trans.* 92:525–530.

Boekema, E. J., B. Hankamer, D. Bald, J. Kruip, J. Nield, A. F. Boonstra, J. Barber, and M. Rögner. 1995. Supramolecular structure of the photosystem II complex from green plants and cyanobacteria. *Proc. Natl. Acad. Sci. U.S.A*. 92:175–179.

Chapados, C., S. Lemieux, and R. Carpentier. 1990. Infrared study of a photosystem II submembrane preparation. *In* Current Research in Photosynthesis. M. Baltscheffsky, editor. Kluwer Academic Publishers, Dordrecht, The Netherlands. I.2.343–346.

Chapados, C., S. Lemieux, and R. Carpentier. 1991. Protein and chlorophyll in photosystem II probed by infrared spectroscopy. *Biophys. Chem.* 39:225–239.

Cornut, I., B. Desbat, J. M. Turlet, and J. Dufourcq. 1996. In situ study by polarization modulated Fourier transform infrared spectroscopy of the structure and orientation of lipids and amphipathic peptides at the air-water interface. *Biophys. J.* 70:305–312.

De Las Rivas, J., J. Klein, and J. Barber. 1995. pH sensitivity of the redox state of cytochrome b559 may regulate its function as a protectant against donor and acceptor side photoinhibition. *Photosynth. Res.* 46: 193–202.

Dieudonné, D., A. Gericke, C. R. Flach, X. Jiang, R. S. Farid, and R. Mendelsohn. 1998. Propensity for helix formation in the hydrophobic peptides $K_2(LA)_x$ (x = 6, 8, 10, 12) in monolayer, bulk, and lipid-

containing phases: infrared and circular dichroism studies. *J. Am. Chem. Soc.* 120:792–799.

Dousseau, F., M. Therrien, and M. Pézolet. 1989. On the spectral subtraction of water from the FT-IR spectra of aqueous solutions of proteins. *Appl. Spectrosc.* 43:538–542.

Fotinou, C., M. Kokkinidis, G. Fritzsch, W. Haase, H. Michel, and D. F. Ghanotakis. 1993. Characterization of a photosystem II core and its three-dimensional crystals. *Photosynth. Res.* 37:41–48.

Gallant, J., H. Lavoie, A. Tessier, G. Munger, R. M. Leblanc, and C. Salesse. 1998. Surface and spectroscopic properties of photosystem II core complex at the nitrogen/water interface. *Langmuir*. 14:3954–3963.

Haag, E., K.-D. Irrgang, E. J. Boekema, and G. Renger. 1990. Functional and structural analysis of photosystem II core complexes from spinach with high oxygen evolution capacity. *Eur. J. Biochem.* 189:47–53.

Haas, H., G. Brezesinski, and H. Möhwald. 1995. X-ray diffraction of a protein crystal anchored at the air/water interface. *Biophys. J.* 68: 312–314.

Hankamer, B., J. Barber, and E. Boekema. 1997. Structure and membrane organization of photosystem II in green plants. *Annu. Rev. Plant Physiol. Plant Mol. Biol.* 48:641–671.

Hanson, O., T. Wydrzynski. 1990. Current perceptions of photosystem II. *Photosynth. Res.* 23:131–162.

He, W.-Z., W. R. Newell, P. I. Haris, D. Chapman, and J. Barber. 1991. Protein secondary structure of the isolated photosystem II reaction center and conformational changes studies by Fourier transform infrared spectroscopy. *Biochemistry*. 30:4552–4559.

Holzenburg, A., T. D. Flint, F. H. Shepherd, and R. C. Ford. 1996. Photosystem II: mapping the locations of the oxygen evolution-enhancing subunits by electron microscopy. *Micron*. 27:121–127.

Jackson, M., and H. H. Mantsch. 1995. The use and misuse of FTIR spectroscopy in the determination of protein structure. *Crit. Rev. Biochem. Mol. Biol.* 30:95–120.

Katz, J. J., R. C. Dougherty, and L. J. Boucher. 1966. Infrared and nuclear magnetic resonance spectroscopy of chlorophyll. *In* The Chlorophylls. L. P. Vernon and G. R. Seely, editors. Academic Press, New York. 185–251.

Kühlbrandt, W., D. N. Wang, and Y. Fujiyoshi. 1994. Atomic model of plant light-harvesting complex by electron crystallography. *Nature.* 367: 614–621.

Lamarche, F. 1988. Une approche permettant de qualifier et de quantifier les interactions lipide-protéine et chlorophyll-protéine à l'interface air-eau. Ph.D. thesis, chapter 2. Université du Québec à Trois-Rivières, Trois-Rivières, Canada.

MacDonald, G. M., R. J. Boerner, R. M. Everly, W. A. Cramer, R. J. Debus, and B. A. Barry. 1994. Comparison of cytochrome b-559 content in photosystem II complexes from spinach and *Synechocystis* species PCC 6803. *Biochemistry*. 33:4393–4400.

Marr, K. M., D. N. Mastronarde, and M. K. Lyon. 1996. Two-dimensional crystals of photosystem II: biochemical characterization, cryoelectron microscopy and localization of the D1 and cytochrome b559 polypeptides. *J. Cell Biol.* 132:823–833.

Morris, E. P., B. Hankamer, D. Zheleva, G. Friso, and J. Barber. 1997. The three-dimensional structure of a photosystem II core complex determined by electron crystallography. *Structure.* 5:837–849.

Nakazato, K., C. Toyoshima, I. Enami, and Y. Inoue. 1996. Two-dimensional crystallization and cryo-electron microscopy of photosystem II. *J. Mol. Biol.* 257:225–232.

Nugent, J. H. A. 1996. Oxygenic photosynthesis: electron transfer in photosystem I and photosystem II. *Eur. J. Biochem.* 237:519–531.

Ocko, B. M., X. Z. Wu, E. B. Sirota, S. K. Sinha, and M. Deutsch. 1994. X-ray reflectivity study of thermal capillary waves on liquid surfaces. *Phys. Rev. Lett.* 72:242–245.

Parratt, L. G. 1954. Surface studies of solids by total reflection of x-rays. *Phys. Rev.* 95:359–369.

Porra, R. J., W. A. Thompson, and P. E. Kriedemann. 1989. Determination of accurate extinction coefficients and simultaneous equations for assaying chorophylls a and b extracted with four different solvents: verification of the concentration of chlorophyll standards by atomic absorption spectroscopy. *Biochim. Biophys. Acta*. 975:384–394.

Rögner, M., E. J. Boekema, and J. Barber. 1996. How does photosystem 2 split water? The structural basis of efficient energy conversion. *Trends Biochem. Sci.* 21:44–49.

Schertler, G. F. X., and P. A. Hargrave. 1995. Projection structure of frog rhodopsin in two crystal forms. *Proc. Natl. Acad. Sci. U.S.A.* 92: 11578–11582.

Seibert, M., M. Dewitt, and L. A. Staehelin. 1987. Multimeric (tetrameric) particles on the luminal surface of freeze-etched photosynthetic membranes. *J. Cell Biol.* 105:2257–2265.

Seidler, A. 1996. The extrinsic polypeptides of photosystem II. *Biochim. Biophys. Acta.* 1277:35–60.

Shuvalov, V. A. 1994. Composition and function of cytochrome b559 in reaction centers of photosystem II of green plants. *J. Bioenerg. Biomembr.* 26:619–626.

Svensson, B., C. Etchebest, P. Tuffery, P. van Kan, J. Smith, and S. Styring. 1996. A model for the photosystem II reaction center core including the structure of the primary donor P_{680}. *Biochemistry*. 35: 14486–14502.

Svensson, B., I. Vass, E. Cedergren, and S. Styring. 1990. Structure of donor side components in photosystem II predicted by computer modelling. *EMBO J.* 9:2051–2059.

Tiede, D. M. 1985. Incorporation of membrane proteins into interfacial films: model membranes for electrical and structural characterization. *Biochim. Biophys. Acta.* 811:357–379.

Trurnit, H. J. 1960. A theory and method for the spreading of protein monolayers. *J. Coll. Sci.* 15:1–13.

Tsiotis, G., T. Walz, A. Spyridaki, A. Lustig, A. Engel, and D. Ghanotakis. 1996. Tubular crystals of a photosystem core complex. *J. Mol. Biol.* 259:241–248.

Uphaus, R. A., J. Y. Fang, R. Picorel, G. Chumanov, J. Y. Wang, T. M. Cotton, and M. Seibert. 1997. Langmuir-Blodgett and x-ray diffraction studies of isolated photosystem II reaction centers in monolayers and multilayers: physical dimensions of the complex. *Photochem. Photobiol.* 65:673–679.

Uzgiris, E. E., and R. D. Kornberg. 1983. Two-dimensional crystallization technique for imaging macromolecules, with application to antigen-antibody-complement complexes. *Nature*. 301:125–129.

van Leeuwen, P. J., M. C. Nieveen, E. J. van de Meent, J. P. Dekker, and H. J. van Gorkom. 1991. Rapid and simple isolation of pure photosystem II core and reaction center particles from spinach. *Photosynth. Res.* 28:149–153.

Vermaas, W. F. J., S. Styring, W. P. Schröder, and B. Andersson. 1993. Photosynthetic water oxidation: the protein framework. *Photosynth. Res.* 38:249–263.

Xiong, J., S. Subramaniam, and Govindjee. 1996. Modeling of the D1/D2 proteins and cofactors of the photosystem II reaction center: implications for the herbicide and bicarbonate binding. *Protein Sci.* 5:2054–2073.

Xu, Q., J. Nelson, and T. M. Bricker. 1994. Secondary structure of the 33 kDa, extrinsic protein of photosystem II: a far-UV circular dichroism study. *Biochim. Biophys. Acta.* 1188:427–431.

Yasuda, Y., Y. Hirata, H. Sugino, M. Kumei, M. Hara, J. Miyake, and M. Fujihara. 1992. Langmuir-Blodgett films of reaction centers of *Rhodopseudomonas viridis*: photoelectric characteristics. *Thin Solid Films.* 210/211:733–735.

Zhang, L.-X., H.-G. Liang, J. Wang, W.-R. Li, and T.-Z. Yu. 1996. Fluorescence and Fourier-transform infrared spectroscopic studies on the role of disulfide bond in the calcium binding in the 33 kDa protein of photosystem II. *Photosynth. Res.* 48:379–384.